International Journal of Minerals, Metallurgy and Materials
Volume 21, Number 10, October 2014, Page 990
DOI: 10.1007/s12613-014-1000-z

Damage prediction of 7025 aluminum alloy during equal-channel angular pressing

M. Ebrahimi[1)], *Sh. Attarilar*[2)], *C. Gode*[3)], *and F. Djavanroodi*[1,4)]

1) Department of Mechanical Engineering, Iran University of Science and Technology, Tehran 16846-13114, Iran
2) Department of Materials Engineering, Sahand University of Technology, Tabriz 51335-1996, Iran
3) School of Denizli Vocational Technology, Program of Machine, Pamukkale University, Denizli 20100, Turkey
4) Department of Mechanical Engineering, Imperial College, London SW7 2AZ, UK
(Received: 12 February 2014; revised: 1 May 2014; accepted: 4 May 2014)

Abstract: Equal-channel angular pressing (ECAP) is a prominent technique that imposes severe plastic deformation into materials to enhance their mechanical properties. In this research, experimental and numerical approaches were utilized to investigate the mechanical properties, strain behavior, and damage prediction of ECAPed 7025 aluminum alloy in various conditions, such as die channel angle, outer corner angle, and friction coefficient. Experimental results indicate that, after the first pass, the yield strength, ultimate tensile strength, and hardness magnitude are improved by approximately 95%, 28%, and 48.5%, respectively, compared with the annealed state, mainly due to grain refinement during the deformation. Finite element analysis shows that the influence of die channel angle is more important than that of outer corner angle or friction coefficient on both the strain behavior and the damage prediction. Also, surface cracks are the main cause of damage during the ECAP process for every die channel angle except for 90°; however, the cracks initiated from the neighborhood of the central regions are the possible cause of damage in the ECAPed sample with the die channel angle of 90°.

Keywords: aluminum alloys; equal-channel angular pressing; materials damage; strain distribution; mechanical properties

1. Introduction

During the last two decades, grain refinement via severe plastic deformation (SPD) methods has been vastly developed by materials science researchers to enhance the mechanical, superplasticity, wear, corrosion, and other properties of metals and alloys for various industrial and medical applications [1–4]. Among the different SPD techniques, such as accumulative roll bonding (ARB) [5], high-pressure torsion (HPT) [6], multi-axial forging/compression (MAF/C) [7], and elliptical cross-section spiral equal-channel extrusion (ECSEE) [8], equal-channel angular pressing (ECAP) [9] has attracted the most attention for fabricating the ultrafine-grained (UFG) and even nanostructured (NS) materials because of its potential of scale-up, more possibilities for industrialization, and low cost and feasibility of set-up [2,9–11].

In 1981, the ECAP process was developed by Segal *et al.* for the first time. This technique imposes large shear plastic strain into the specimen by pushing it through a die that consists of two channels with the same cross-section, meeting at an angle to each other, namely the die channel angle (Φ) [2]. The shear plastic strain (γ) and effective plastic strain (ε_{eq}) in the frictionless condition are represented in Eqs. (1) and (2) [2,12], respectively.

$$\gamma = 2\cot\left(\frac{\Phi+\Psi}{2}\right)+\Psi\csc\left(\frac{\Phi+\Psi}{2}\right) \tag{1}$$

$$\varepsilon_{eq} = \frac{N}{\sqrt{3}}\cdot\left[2\cot\left(\frac{\Phi+\Psi}{2}\right)+\Psi\csc\left(\frac{\Phi+\Psi}{2}\right)\right] \tag{2}$$

where N is the number of passes, Φ the die channel angle, and Ψ the outer corner angle.

Since the cross-section of the two channels is the same, the ECAPed sample after the first pass can be reinserted into the entrance channel and pushed again through the die. As

Corresponding author: M. Ebrahimi E-mail: mebrahimi@iust.ac.ir

known, the repeated pressing through the die accumulates the sufficient plastic strain to achieve the desired properties [13]. The finite element method (FEM) has been widely used to examine the material deformation behavior of the ECAP process [14–18]. By considering the previous studies carried out on the ECAP process via the FEM approach, one can see that most studies have been carried out in a two-dimensional (2D) plane strain condition [19–23]. As an example, 2D FEM investigation of Nagasekhar *et al.* showed that the ECAP process proceeded in three steps for the acute die channel angles, in comparison with only two steps for the case of Φ =90°. Also, formation of a corner gap, which was often the major disadvantage in the case of the 90° die channel angle, was not encountered for the acute die channel angles. In addition, back-pressure punch is required for the acute die channel angles [24]. Recently, Mahallawy *et al.* [25], Lu *et al.* [26], and Ghazani and Eghbali [27] have carried out some three-dimensional (3D) analyses to investigate the effects of various ECAP parameters on the strain behavior, damage prediction, and required punch load after the ECAP process along the longitudinal and transversal directions. Simply, it can be said that the effective strain magnitude, strain distribution uniformity, required pressing force, and damage anticipation are affected by the ECAP parameters, such as die channel angle, outer corner angle, friction coefficient, processing routes, back pressure, billet size, strain rate sensitivity, processing temperature, pass number, material response, and kind of solution treatment [14–28]. The research by Figueiredo *et al.* [29] showed that the high levels of damage may accumulate in the material, exhibiting the strain-hardening behavior, which may lead to billet segmentation, whereas in the near-perfect plastic condition, the cracking occurs only on the upper surfaces of the billets and these cracks are reasonably stable. From the previous studies, it can be concluded that the level of the imposed plastic strain is improved by applying an acute die channel angle or adding a friction coefficient value. Also, a lower die channel angle or higher friction coefficient leads to fill the outer corner of the die completely [23,30]. The investigation by Oruganti *et al.* [31] represented that a better strain behavior of an ECAPed sample was obtained by applying high back pressure with low friction for the ECAP process. Also, route B_C, in which the sample is rotated with the angle of 90° along the longitudinal axis between each pass of process, gives a better strain dispersal homogeneity, compared with the other routes for the die channel angle of 90° [25].

Although several investigations have been carried out on the effects of ECAP process parameters, there is a lack of information about their influences on the strain distribution uniformity and damage prognostication after the ECAP process. In this research, the numerical investigations using DEFORM-3D software were carried out on the Al7025 billet to explore the effects of die channel angle, outer corner angle, and friction coefficient on the effective strain magnitude, strain distribution uniformity, and damage anticipation after the first pass of the ECAP process at room temperature. Also, the mechanical properties of Al7025 before and after the process were obtained and compared.

2. Experimental

An equal-channel angular pressing die with the channel angle of 90°, outer corner angle of 17°, and channel diameter of 20 mm was designed and manufactured. The die and punch were made of hot work tool steel (AISI H13) to prevent any deformation during the process. A 7025 aluminum alloy was prepared as a test material with the length and diameter of 140 mm and 20 mm, respectively. The chemical composition of Al7025 is listed in Table 1. Before the ECAP process, all Al7025 billets were annealed at 475°C for 3 h, and then slowly cooled in the furnace. ECAP operation was carried out using a hydraulic press with a punch speed of 1 mm/s. Also, the molybdenum disulfide was used as a lubricant to reduce frictional effects during operation. The ECAP die and the deformed material after one pass are shown in Fig. 1.

Table 1. Chemical composition of 7025 aluminum alloy wt%

Al	Zn	Mg	Mn	Fe	Si	Cr	Cu	Ti
92.60	4.13	1.32	0.60	0.37	0.31	0.28	0.17	0.11

Fig. 1. ECAP die set-up and Al7025 sample after the first pass.

Tensile and micro-hardness measurements were carried out to investigate the magnitude of strength and hardness for both as-received and ECAPed conditions. The average reading of five Vickers micro-hardness (Hv) measurements from the central region of the sample's cross-section was

reported. The hardness tests were performed according to ASTM E10–04 with a force of 0.588 N for a dwell time of 20 s. In addition, the microstructure evaluation using optical microscopy (OM) was employed to confirm the grain-size refining after the ECAP process.

3. Finite element modeling

Commercial three-dimensional DEFORM-3D-V10.0 software was used for the finite element modeling. The die and punch were assumed to be discretely rigid, meaning that there was no deformation during the process because of their strength and rigidity (hot work tool steel, H13) compared with the sample material (Al7025-O). The process was carried out in the ambient temperature. Also, the heat generation was ignored during the operation. In addition, the magnitude of ram speed was equal to 1 mm/s, which is the same as in the experimental work. The value of shear friction coefficient (m) was considered to be 0.12 [32], obtained from a ring compression test (outer diameter : inner diameter : height = 6:3:2) and calibrated with the curves recommended by Male and Cockcroft [33]. To import material properties to the FEM software, a true stress–strain tensile curve was obtained according to ASTM B557M (2010), and the curve fitting was also carried out using the Hollomon relationship, as shown in Fig. 2. Furthermore, the dimension of the simulated Al7025 sample was similar to the experimental one, i.e., 140 mm in length and 20 mm in diameter. The mesh sensitivity diagram for the billet was attained, and then the optimum element size was found to be 0.7 mm; as shown in Fig. 3. Adaptive meshing and automatic re-meshing were applied and justified for all simulations to prevent the failure of mesh during large deformation and to reduce computation time.

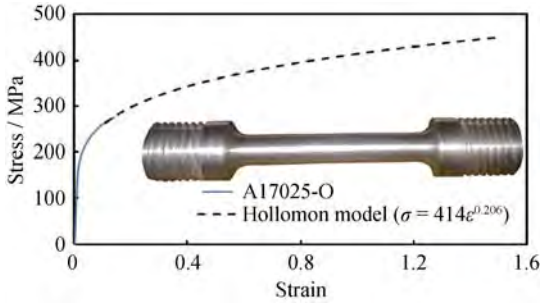

Fig. 2. True stress–strain curve of the annealed Al7025 billet before ECAP operation.

The effective strain magnitude and its uniformity were investigated for the whole of the ECAPed sample and also at five separate equally spaced planes parallel to the billet cross-section with 20 mm distance between them, as represented in Fig. 4(a). These planes were nominated as planes 1, 2, 3, 4, and 5, in which planes 1 and 5 were placed at a distance of 30 mm from the head and the tail part, respectively.

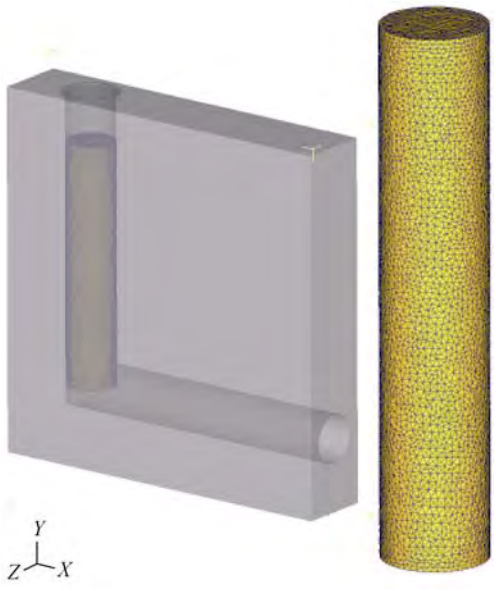

Fig. 3. Billet volume meshing system before ECAP process.

Furthermore for these planes, 21 elements at each plane were selected to study the effective strain magnitude and its homogeneity behavior, as shown in Fig. 4(b). All these chosen points were away from the circumferential locations to remove the frictional effects between the die and the billet on strain behavior. As represented in Fig. 4(b), one point is located at the center of plane, and eight and twelve points are at the periphery of the small and large assumed circles, with an angular distance of 45° and 30°, respectively. There are two factors representing the uniformity of effective strain distribution, the inhomogeneity factor (IF) in Eq. (3) and the inhomogeneity index (C_i) in Eq. (4) [34–35]. Low magnitudes of IF or C_i indicate the better uniformity of effective strain distribution is achieved [35].

$$\mathrm{IF} = \sqrt{\left[\sum_{i=1}^{n}\left(\varepsilon_i - \varepsilon_{\mathrm{ave}}\right)^2\right]} \Big/ (n-1) \tag{3}$$

$$C_i = \frac{\varepsilon_{\max} - \varepsilon_{\min}}{\varepsilon_{\mathrm{ave}}} \tag{4}$$

where ε_i, $\varepsilon_{\max}$, $\varepsilon_{\min}$, $\varepsilon_{\mathrm{ave}}$, and n are the strain value of the ith element, the maximum effective strain value, the minimum effective strain value, the mean effective strain value, and the number of elements, respectively. The IF is a better tool for representing the strain dispersal homogeneity, because it includes the effective strain magnitude for all the elements of sample. Hence, IF was utilized in this research.

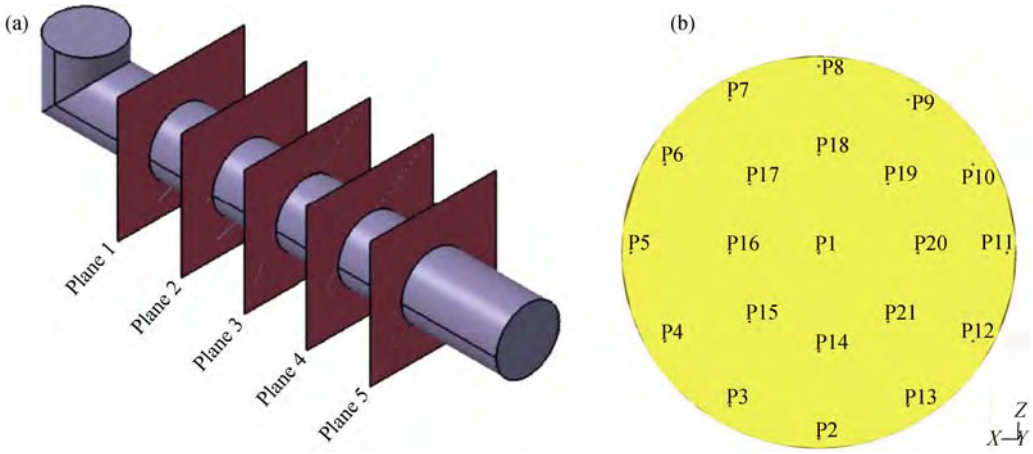

Fig. 4. Locations of 5 cross-sectional planes (a) and 21 elements to measure strain behavior (b).

In this research, a 7025 aluminum alloy billet was numerically ECAPed up to one pass with various parameters, including the die channel angles of 70°, 90°, and 110°; the outer corner angles of 0°, 17°, and 50°; and the friction coefficients of 0.001, 0.01, 0.12, 0.2, and 0.3. The effects of the above parameters on strain behavior, including the magnitude of effective strain (ES) and the uniformity of effective strain distribution (IF), were investigated. In addition, the damage magnitude and its distribution after the ECAP process for various parameters were obtained and discussed.

4. Results and discussion

4.1. Strain behavior

Table 2 lists the ES and IF values for the entire ECAPed sample under the various conditions in the ECAP process (Φ, Ψ, and m). Also, the effective strain contours of the ECAPed Al7025 sample after the one-pass process are shown in Fig. 5.

Table 2. Effective strain (ES) value and inhomogeneity factor (IF) under the various conditions in ECAP process

ECAPed sample No.	Parameters			Outputs	
	Φ / (°)	Ψ / (°)	m	ES	IF
1	90	17	0.12	0.909	0.477
2	70	17	0.12	1.530	0.869
3	110	17	0.12	0.628	0.294
4	90	0	0.12	0.987	0.433
5	90	50	0.12	0.896	0.392
6	90	17	0.001	0.852	0.383
7	90	17	0.01	0.861	0.399
8	90	17	0.2	1.050	0.543
9	90	17	0.3	1.310	0.742

Although the high die channel angles led to lower effective strain magnitudes, a better strain distribution uniformity was attained at the deformed samples. About 31% and 38% reductions were obtained for the effective strain value and inhomogeneity factor, respectively, using Φ = 110° instead of 90°, while all other boundary conditions used in the simulation were kept similar. On the other hand, lower effective strain magnitude with better strain dispersal homogeneity was obtained by applying a higher outer corner angle. As an example, for a similar simulation condition except using Ψ = 50° instead of Ψ = 17°, there were approximately 1.4% and 18% reductions at the ES and IF values, respectively. It was found that the effect of die channel angle on strain behavior was greater than that of the outer corner angle. The numerical examination of the friction coefficient effect indicated that a lower effective strain value with better strain-dispersal homogeneity could be obtained using a well-lubricated ECAP operation. For example, the magnitudes of ES and IF increased to 1.310 and 0.742 from 0.852 and 0.383 by utilizing m = 0.3 instead of m = 0.001, respectively. Fig. 6 compares the influences of ECAP parameters on the effective strain magnitude and inhomogeneity factor. It can be seen that the influence of die channel angle is considerably greater than that of both outer corner angle and friction coefficient on the effective strain magnitude.

In addition, Table 3 lists the magnitudes of ES after one pass of ECAP process of the Al7025 billet. As can be seen, these findings are in good agreement with the above results. The best and the worst strain behavior belong to the ECAP processes with the conditions of No. 2 (Φ = 70°, Ψ = 17°, and m = 0.12) and No. 3 (Φ = 110°, Ψ = 17°, m = 0.12), respectively. This result indicated that the effect of die channel angle was the most prominent factor on the strain behavior of the ECAPed billet compared with the outer corner angle and friction coefficient. A comparison of the effective strain contour at the cross-section of the ECAPed Al7025 billet in plane 3 for No. 2 (Φ = 70°, Ψ = 17°, m = 0.12) and No. 3 (Φ = 110°, Ψ = 17°, m = 0.12) is shown in Fig. 7.

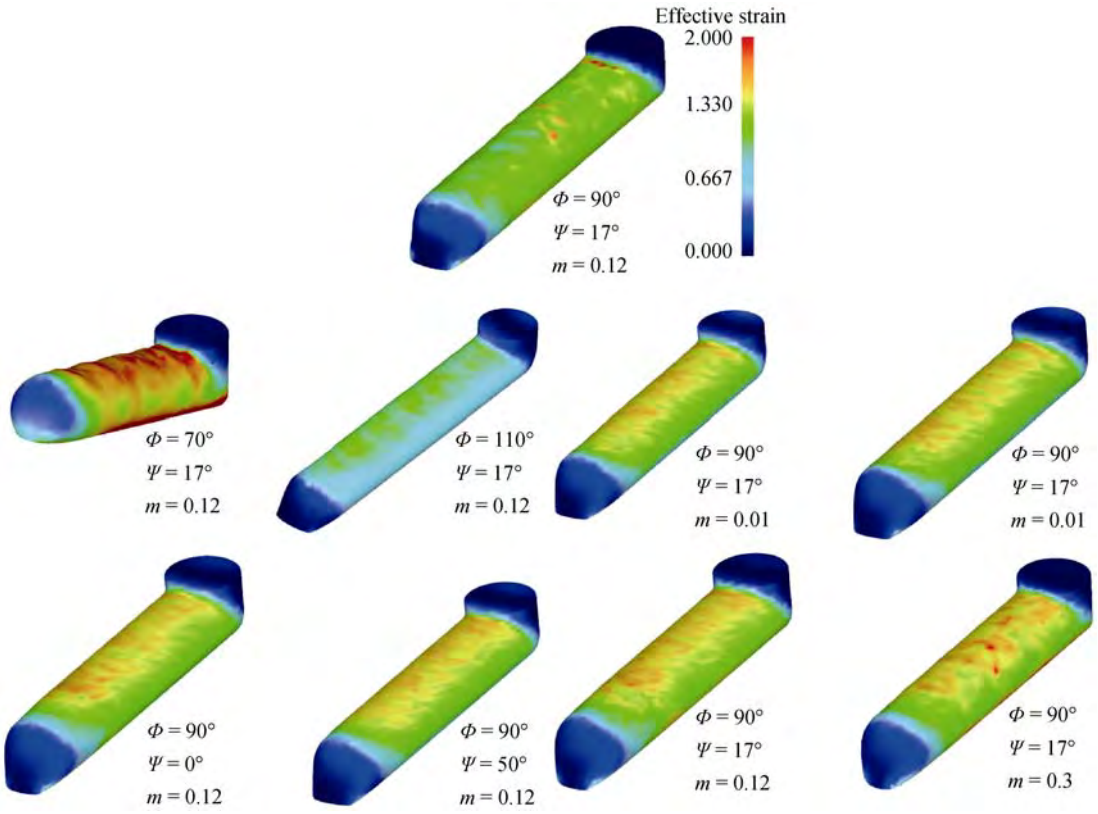

Fig. 5. Effective strain contour of the ECAPed Al7025 billet for various parameters

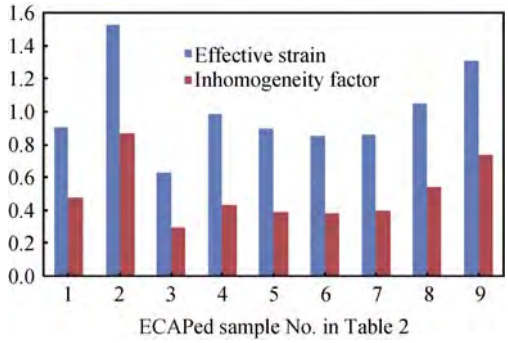

Fig. 6. Effective strain and inhomogeneity factor magnitudes for various parameters of ECAP operation.

4.2. Damage prediction

The development and tendency of surface cracks are one of the major problems for the application of subsequent passes in ECAP and other SPD methods. In this research, the Cockcroft–Latham damage model was numerically applied to examine the fracture of Al7025 billet after the ECAP process with various parameters. As known, the fracture is related to the development of tensile maximum principle stresses during the deformation process. The Cockcroft–Latham damage criterion is expressed as the following equation [27].

Table 3. Effective strain magnitude for each of the five planes shown in Fig. 4 for various ECAP parameters

No.	Φ, Ψ, m	Effective strain				
		Plane 1	Plane 2	Plane 3	Plane 4	Plane 5
1	90°, 17°, 0.12	0.846	1.173	1.173	1.151	1.035
2	70°, 17°, 0.12	1.286	1.661	1.838	1.862	1.41
3	110°, 17°, 0.12	0.695	0.793	0.743	0.734	0.726
4	90°, 0°, 0.12	1.001	1.063	1.029	1.016	1.109
5	90°, 50°, 0.12	0.956	0.972	0.984	0.971	1.021
6	90°, 17°, 0.001	0.903	0.936	0.958	0.973	0.932
7	90°, 17°, 0.01	0.912	0.974	1.007	1.09	0.981
8	90°, 17°, 0.2	1.003	1.085	1.098	1.122	1.088
9	90°, 17°, 0.3	1.246	1.433	1.525	1.528	1.298

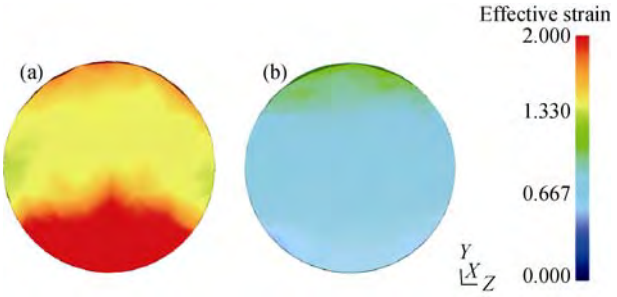

Fig. 7. Effective strain contour at the cross-sectional plane 3 of the ECAPed sample after one-pass process: (a) Φ = 70°, Ψ = 17°, and m = 0.12; (b) Φ = 110°, Ψ = 17°, and m = 0.12.

$$C_N = \int_0^{\varepsilon_f} \bar{\sigma}\left(\frac{\sigma_m}{\bar{\sigma}}\right) d\bar{\varepsilon} \quad (5)$$

where C_N is a constant indicating the critical condition for initiation of fracture, σ_m the maximum principle stress, $\bar{\varepsilon}$ and $\bar{\sigma}$ the effective strain and the effective stress, respectively, and the integral is calculated from zero strain to the fracture strain (ε_f). Considering the above equation, it can be said that the fracture occurs when the damage factor reaches the critical value, which has been assumed to be equal to 0.5.

The damage contour of the all simulated ECAPed samples after the first pass is represented in Fig. 8 at the extruded and transversal planes (plane 3). In addition, the average magnitudes of damage are shown in Fig. 9.

As can be seen in Fig. 9, the maximum damage value of deformed Al7025 is related to the ECAP process with the die channel angle, outer corner angle, and friction coefficient of 70°, 17°, and 0.12, respectively. This finding is clearly shown in Fig. 8. The high damage magnitudes are concentrated in a narrow region located at the bottom surface, parallel to the longitudinal axis of the sample, and distinguished by red color. On the other hand, the minimum damage value belongs to the ECAPed sample with Φ = 110°, Ψ = 17°, and m =0.12. It is also found that the effect of die channel angle is considerably greater than that of either the outer corner angle or the friction coefficient on the damage magnitude. There is an approximately 17% reduction in the damage value using the lower friction coefficient (0.001) instead of the higher one (0.3). Furthermore, only about 3% improvement at the damage magnitude is achieved using a higher outer corner angle (50°) compared with the sharp outer corner one. In addition, Fig. 10 represents the damage

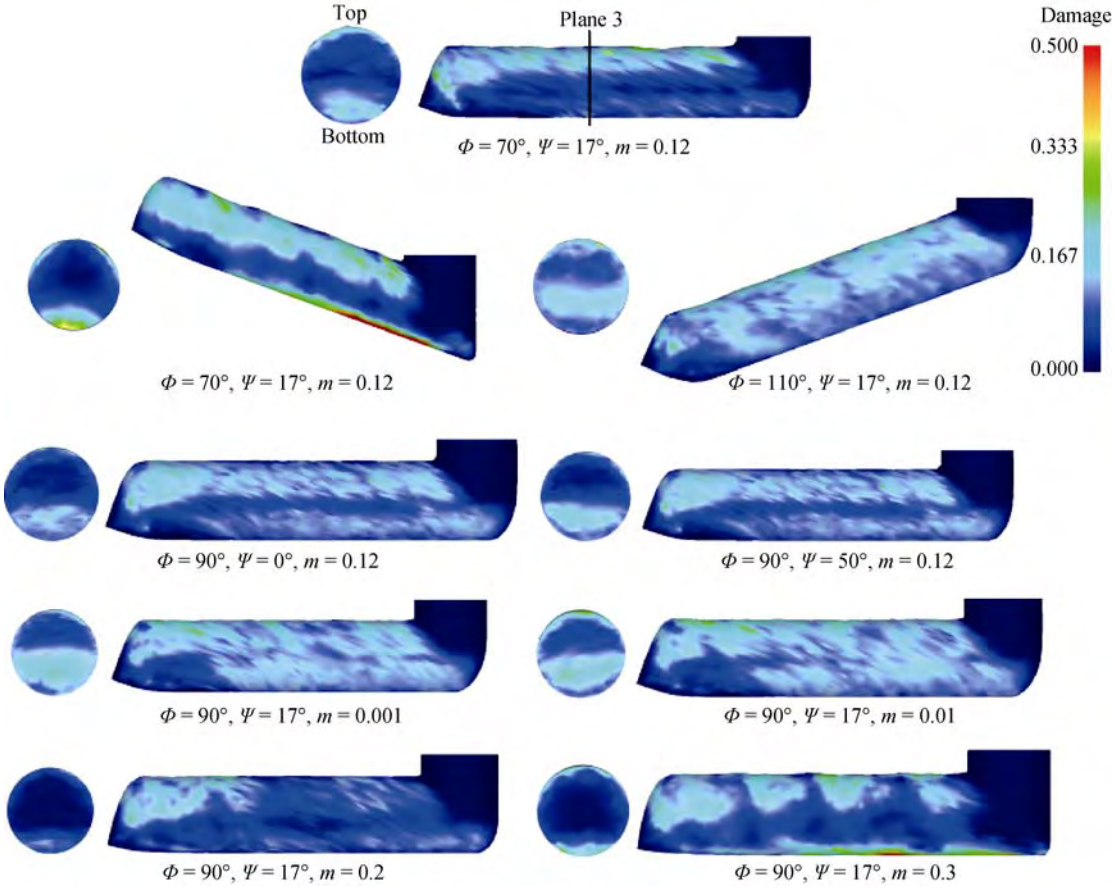

Fig. 8. Damage contour of the deformed Al7025 billet for various ECAP parameters at the extruded and transversal planes.

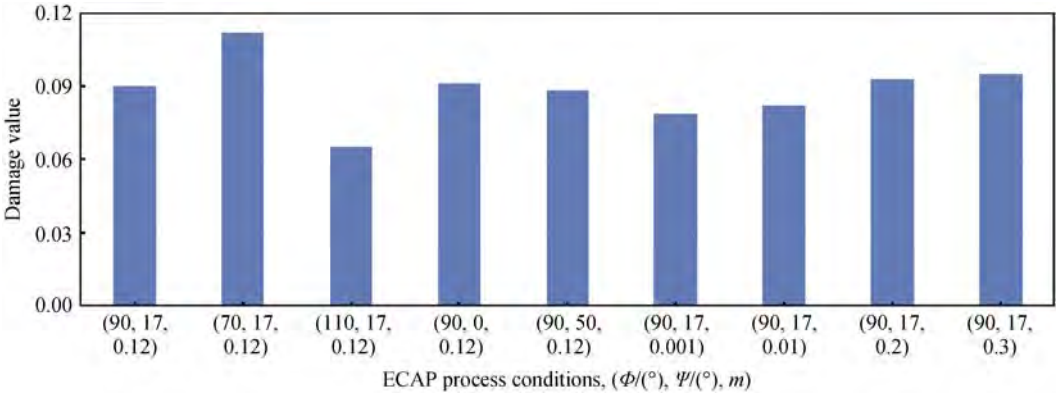

Fig. 9. Average damage magnitudes for ECAPed sample with various parameters.

value curves in three ECAP process conditions at plane 3 from top to bottom. These three circumstances are (Φ = 70°, Ψ = 17°, m = 0.12), (Φ = 110°, Ψ = 17°, m = 0.12), and (Φ = 90°, Ψ = 17°, m = 0.12), corresponding to the maximum damage value, the minimum damage value, and the basic conditions (the same as the experimental work), respectively, of the ECAPed Al7025 billet. The only parameter altered is the die channel angle. It can be seen that the area of the deformed sample with the highest damage value is intensively related to the die channel angle. It is found that the highest damage magnitude is attained at the bottom surface for Φ < 90° and at the top surface for Φ > 90°, respectively, after one pass of the process. It is believed that the formation of cracks at the top surface of the ECAPed sample with a die channel angle of 70° is more likely than at the bottom surface of the ECAPed sample with a die channel angle of 110°. Also, the lowest damage value is obtained at the center of the vertical line (top to bottom), irrespective of the die channel angle magnitude. In the case of the ECAP process with the die channel angle of 90°, it can be seen that the highest damage value is attained in the region with the distance of 4 mm from the bottom surface. On the other hand, the uniformity of damage distribution is increased by increasing the die channel angle. From Fig. 10, the standard deviations (SD) of damage magnitudes along the top-to-bottom line in the middle plane of the ECAPed sample are 0.0990, 0.0525, and 0.0370 for the die channel angles of 70°, 90°, and 110°, respectively. It is evident that the reduction of die channel angle from 110° to 70° results in a 63% increase of the SD value, indicating that a higher die channel angle gives a more uniform damage distribution in the ECAPed billet. It is also noted that surface cracks are the main cause of damage during the ECAP process for $\Phi \neq 90°$, but the cracks which are initiated from the neighborhood of the central regions are the possible cause of damage in the ECAPed sample with Φ = 90°.

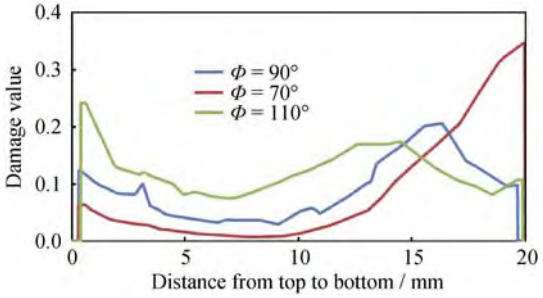

Fig. 10. Damage curve from top to bottom for three ECAP process conditions.

4.3. Mechanical and microstructural properties

The mechanical and microstructural evaluations of the aluminum alloy before and after the ECAP process are represented in Fig. 11, and the results are listed in Table 4. As

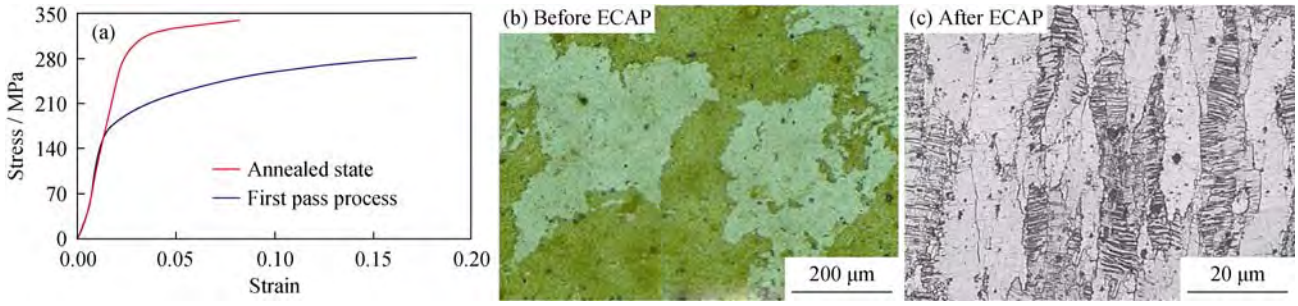

Fig. 11. True stress–strain curve (a) and optical microscopy images of the Al7025 billet before (b) and after (c) the first pass of the ECAP process.

Table 4. Mechanical properties of the aluminum alloy before and after the ECAP process

Mechanical properties	Before ECAP process	After ECAP process
Yield strength (YS) / MPa	143	279
Ultimate tensile strength (UTS) / MPa	258	331
Vickers micro-hardness, Hv	72	107
Elongation to failure (El) / %	17	8.2

can be seen, a considerable enhancement is observed after the first pass of ECAP for the aluminum alloy in which the magnitude of yield strength (YS), ultimate tensile strength (UTS), and hardness are increased to 279 MPa, 331 MPa, and Hv 107 from 143 MPa, 258 MPa, and Hv 72, respectively. This enhancement in strength is related to grain refinement according to the Hall–Petch relationship. The magnitude of average grain size before the ECAP process is about 180 μm (annealed condition). Also, elongated grains with the width of approximate 7 μm are formed after the first pass of the ECAPed process at the flow plane (*Y* plane). This confirms the grain refinement of 7025 aluminum alloy during the ECAP method.

5. Conclusions

Finite element analysis was used to investigate the strain and damage behaviors of ECAPed 7025 aluminum alloy after the first pass of equal-channel angular pressing (ECAP) with various parameters, including die channel angle, outer corner angle, and friction coefficient. In addition, an ECAP die with the die channel and outer corner angles of 90° and 17°, respectively, was designed and manufactured to study the hardness behavior, tensile strength, and grain size of the deformed Al7025 billet compared with the annealed samples and to validate the FEM analysis.

(1) Die channel angle is a notably more important factor than either outer corner angle or friction coefficient on both the strain and damage behavior.

(2) Both large die channel and outer corner angles lead to the fabrication of an ECAPed billet with the low damage value, less effective strain magnitude, and improved strain distribution homogeneity.

(3) The crack formation possibility in the ECAPed specimen is reduced by the utilization of lubricant. In addition, better strain distribution homogeneity and lower effective strain values are obtained in this way.

(4) Surface cracks are the main cause of damage during the ECAP process for die channel angle $\neq 90°$; however, the near-center-region cracks are the possible cause of damage in the ECAPed sample for die channel angle = 90°.

(5) About 95%, 28%, and 48.5% enhancements are attained at the yield strength, ultimate tensile strength, and Vickers hardness value, respectively, after the first pass of the ECAP process in Al7025 alloy. Also, the microstructural observations show the grain refinement during this deformation.

Acknowledgements

This work was financially supported by the Scientific and Technological Research Council of Turkey (TÜBITAK) under the 2216 Research Fellowship Program for Foreign Citizens.

References

[1] R.Z. Valiev, R.K. Islamgaliev, and I.V. Alexandrov, Bulk nanostructured materials from severe plastic deformation, *Prog. Mater Sci.*, 45(2000), p. 103.

[2] R.Z. Valiev and T.G. Langdon, Principles of equal-channel angular pressing as a processing tool for grain refinement, *Prog. Mater. Sci*., 51(2006), p. 881.

[3] A. Azushima, R. Kopp, A. Korhonen, D.Y. Yang, F. Micari, G.D. Lahoti, P. Groche, J. Yanagimoto, N. Tsuji, A. Rosochowski, and A. Yanagida, Severe plastic deformation (SPD) processes for metals, *CIRP Ann. Manuf. Technol*., 57(2008), p. 716.

[4] T.G. Langdon, Twenty-five years of ultrafine-grained materials: achieving exceptional properties through grain refinement, *Acta Mater.*, 61(2013), p. 7035.

[5] M. Shaarbaf and M.R. Toroghinejad, Nano-grained copper strip produced by accumulative roll bonding process, *Mater. Sci. Eng. A*, 473(2008), p. 28.

[6] A.P. Zhilyaev and T.G. Langdon, Using high-pressure torsion for metal processing: Fundamentals and applications, *Prog. Mater. Sci*., 53(2008), p. 893.

[7] Q. Chen, D.Y. Shu, C.K. Hu, Z.D. Zhao, and B.G. Yuan, Grain refinement in an as-cast AZ61 magnesium alloy processed by multi-axial forging under the multitemperature processing procedure, *Mater. Sci. Eng. A*, 541(2012), p. 98.

[8] C.P. Wang, F.G. Li, Q.H. Li, and L. Wang, Numerical and experimental studies of pure copper processed by a new severe plastic deformation method, *Mater. Sci. Eng. A*, 548(2012), p. 19.

[9] V.M. Segal, Equal channel angular extrusion: from macromechanics to structure formation, *Mater. Sci. Eng. A*, 271(1999), p. 322.

[10] B.Q. Han and T.G. Langdon, Improving the high-temperature mechanical properties of a magnesium alloy by equal-channel angular pressing, *Mater. Sci. Eng. A*, 410-411(2005), p. 435.

[11] F. Akbaripanah, F. Fereshteh-Saniee, R. Mahmudi, and H.K. Kim, The influences of extrusion and equal channel angular pressing (ECAP) processes on the fatigue behavior of AM60

magnesium alloy, *Mater. Sci. Eng. A*, 565(2013), p. 308.

[12] W.J. Zhao, H. Ding, Y.P. Ren, S.M. Hao, J. Wang, and J.T. Wang, Finite element simulation of deformation behavior of pure aluminum during equal channel angular pressing, *Mater. Sci. Eng. A*, 410-411(2005), p. 348.

[13] A. Rebhi, T. Makhlouf, N. Njah, Y. Champion, and J.P. Couzinié, Characterization of aluminum processed by equal channel angular extrusion: effect of processing route, *Mater. Charact*., 60(2009), p. 1489.

[14] C.J. Luis-Pérez, R. Luri-Irigoyen, and D. Gastón-Ochoa, Finite element modelling of an Al–Mn alloy by equal channel angular extrusion (ECAE), *J. Mater. Process. Technol*., 153-154(2004), p. 846.

[15] F.Q. Yang, A. Saran, and K. Okazaki, Finite element simulation of equal channel angular extrusion, *J. Mater. Process. Technol*., 166(2005), p. 71.

[16] H.S. Kim, M.H. Seo, and S.I. Hong, On the die corner gap formation in equal channel angular pressing, *Mater. Sci. Eng. A*, 291(2000), p. 86.

[17] S. Dumoulin, H.J. Roven, J.C. Werenskiold, and H.S. Valberg, Finite element modeling of equal channel angular pressing: Effect of material properties, friction and die geometry, *Mater. Sci. Eng. A*, 410-411(2005), p. 248.

[18] S.B. Xu, G.Q. Zhao, X.W. Ma, and G.C. Ren, Finite element analysis and optimization of equal channel angular pressing for producing ultra-fine grained materials, *J. Mater. Process. Technol.*, 184(2007), p. 209.

[19] H.S. Kim, M.H. Seo, and S.I. Hong, Plastic deformation analysis of metals during equal channel angular pressing, *J. Mater. Process. Technol*., 113(2001), p. 622.

[20] S.C. Yoon, P. Quang, S.I. Hong, and H.S. Kim, Die design for homogeneous plastic deformation during equal channel angular pressing, *J. Mater. Process. Technol*., 187-188(2007), p. 46.

[21] B.S. Moon, H.S. Kim, and S.I. Hong, Plastic flow and deformation homogeneity of 6061 Al during equal channel angular pressing, *Scripta Mater.*, 46(2002), p. 131.

[22] S.C. Yoon, H.G. Jeong, S. Lee, and H.S. Kim, Analysis of plastic deformation behavior during back pressure equal channel angular pressing by the finite element method, *Comput. Mater. Sci*., 77(2013), p. 202.

[23] A.V. Nagasekhar, Y. Tick-Hon, and H.P. Seow, Deformation behavior and strain homogeneity in equal channel angular extrusion/pressing, *J. Mater. Process. Technol.*, 192-193(2007), p. 449.

[24] V.N. Anumalasetty, T. Yip, S. Li, and H.P. Seow, Effect of acute tool-angles on equal channel angular extrusion/pressing, *Mater. Sci. Eng. A*, 410-411(2005), p. 269.

[25] N.E. Mahallawy, F.A. Shehata, M.A.E. Hameed, M.I.A.E. Aal, and H.S. Kim, 3D FEM simulations for the homogeneity of plastic deformation in Al–Cu alloys during ECAP, *Mater. Sci. Eng. A*, 527(2010), p. 1404.

[26] S.K. Lu, H.Y. Liu, L. Yu, Y.L. Jiang, and J.H. Su, 3D FEM simulations for the homogeneity of plastic deformation in aluminum alloy HS6061-T6 during ECAP, *Procedia Eng*., 12(2011), p. 35.

[27] M.S. Ghazani and B. Eghbali, Finite element simulation of cross equal channel angular pressing, *Comput. Mater. Sci*., 74(2013), p. 124.

[28] X.N. Zhang, L. Hua, and Y.X. Liu, FE simulation and experimental investigation of ZK60 magnesium alloy with different radial diameters processed by equal channel angular pressing, *Mater. Sci. Eng. A*, 535(2012), p. 153.

[29] R.B. Figueiredo, P.R. Cetlin, and T.G. Langdon, The evolution of damage in perfect-plastic and strain hardening materials processed by equal-channel angular pressing, *Mater. Sci. Eng. A*, 518(2009), p. 124.

[30] F. Djavanroodi and M. Ebrahimi, Effect of die channel angle, friction and back pressure in the equal channel angular pressing using 3D finite element simulation, *Mater. Sci. Eng. A*, 527(2010), p. 1230.

[31] R.K. Oruganti, P.R. Subramanian, J.S. Marte, M.F. Gigliotti, and S. Amancherla, Effect of friction, backpressure and strain rate sensitivity on material flow during equal channel angular extrusion, *Mater. Sci. Eng. A*, 406(2005), p. 102.

[32] F. Djavanroodi and M. Ebrahimi, Effect of die parameters and material properties in ECAP with parallel channels, *Mater. Sci. Eng. A*, 527(2010), p. 7593.

[33] A.T. Male and M.G. Cockcroft, A method for the determination of the coefficient of friction of metals under condition of bulk plastic deformation, *J. Inst. Met.*, 93(1964), p. 38.

[34] H.J. Hu, D.F. Zhang, and F.S. Pan, Die structure optimization of equal channel angular extrusion for AZ31 magnesium alloy based on finite element method, *Trans. Nonferrous Met. Soc. China*, 20(2010), p. 259.

[35] P. Venkatachalam, S.R. Kumar, B. Ravisankar, V.T. Paul, and M. Vijayalakshmi, Effect of processing routes on microstructure and mechanical properties of 2014 Al alloy processed by equal channel angular pressing, *Trans. Nonferrous Met. Soc. China*, 20(2010), p. 1822.